AN ABSTRACT OF THE THESIS OF

<u>Praveen Prabha</u> for the degree of <u>Master of Science</u> in <u>Electrical and Computer Engineering</u> presented on <u>March 7, 2014</u>.

Title: <u>Design Techniques For VCO Based Digital Sensor Readout Circuits</u>

Abstract approved: _____

Pavan Kumar Hanumolu

Sensors find a variety of applications in portable electronics, automotive and biomedical solutions. The demand for low power and high dynamic range makes the design of digital sensor readout circuits quite challenging. Traditionally, these circuits are realized using amplifiers with passive feedback or precision analog comparators which are power hungry and not amenable to technology scaling.

This thesis presents design techniques for a low power, amplifier-free, digital sensor current readout circuit. It is realized using an implicit passive integrator, VCO-based quantizer, and mostly digital circuits. A digital IIR filter is used to increase the loop gain and bias the sensor accurately across a wide range of values. Fabricated in a 0.18μm CMOS process, the prototype readout circuit achieves $900p$A accuracy over an input current range of 4μA, consumes a total of 77.8μA current, and occupies an active area of 0.36mm^2.

Design Techniques For VCO Based Digital Sensor Readout Circuits

by

Praveen Prabha

A THESIS

submitted to

Oregon State University

in partial fulfillment of
the requirements for the
degree of

Master of Science

Presented March 7, 2014
Commencement June 2014

Master of Science thesis of <u>Praveen Prabha</u> presented on <u>March 7, 2014</u>.

APPROVED:

_____

Major Professor, representing Electrical and Computer Engineering

_____

Director of the School of Electrical Engineering and Computer Science

_____

Dean of the Graduate School

I understand that my thesis will become part of the permanent collection of Oregon State University libraries. My signature below authorizes release of my thesis to any reader upon request.

_____

Praveen Prabha, Author

ACKNOWLEDGEMENTS

TABLE OF CONTENTS

LIST OF FIGURES

LIST OF FIGURES (Continued)

LIST OF TABLES

CHAPTER 1

INTRODUCTION

Sensors play an increasingly important role these days as more and more electronics find their way into our lives. In portable devices like mobile phones, high performance CMOS image sensors are used for camera [1], and proximity sensors are used to turn off backlight while on call. These devices also contain ambient light sensors (ALS) to adjust display power depending on ambient light conditions thus improving battery life. Medical applications use light sensors for pulse oximetry which is a
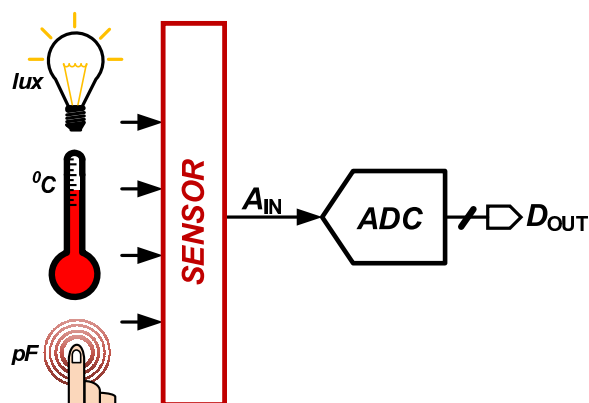
Figure 1.1: Generic block diagram of a digital sensor readout circuit.

non-invasive method for monitoring oxygen levels [2] and photo-plethysmographic biosensing to get a volumetric measurement of an organ [3]. Automotive industry demands a slew of sensors which assists the driver for parking and driving. In all of these applications, a digital sensor readout circuit is used to convert the sensor output to a digital signal for further processing. Figure 1.1 shows a generic block diagram of a typical digital sensor readout circuit.

The rising demand for portable devices and higher integration of sensors necessitate readout circuits with ultra low power consumption and small area. Moreover, majority of the sensors give out a signal that can have a large variation. For instance, Figure 1.2 shows the photocurrent variation taken from the datasheet of an ALS chip [4]. The input to the sensor is the ambient light measured in illuminance
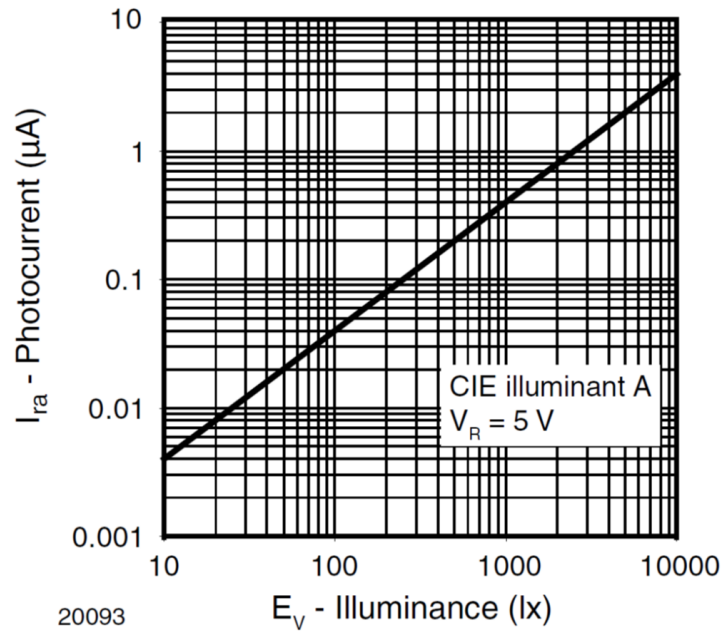
Figure 1.2: Photocurrent variation of a typical light sensor (external photodiode).

(lux) and the output of the sensor is a current which ranges from nA to μA. It can be seen that the output dynamic range is more than $60\,$dB and the readout circuits used for such an application should have large dynamic range. In addition to these constraints at system level, some of these sensors need external biasing. The front end circuit design of their readout circuits should be capable of providing the required bias. For example, the ALS sensor shown in Figure 1.2 needs to be reverse biased at around 5V for right operation.

1.1   Scope of this work

Majority of the existing current sensing methods either employ trans-impedance amplifiers with resistive feedback [2] or precision zero crossing detectors [5] along with an ADC to generate the digital output. However, these classical approaches require large resistors/capacitors, carefully designed analog amplifiers/comparators which are not amenable to technology scaling and consumes large power. In this thesis, a highly digital approach is proposed in which a voltage-controlled oscillator (VCO) combined with synthesized digital logic is used in place of a conventional readout circuit to precisely convert the sensor current to digital output. The proposed architecture is also capable of providing an accurate and stable biasing for the sensor if needed. Moreover, the architecture being highly digital, will benefit from improved time resolution in future technology nodes and allow easy portability without much redesign. The prototype achieves $900p$A accuracy for an input current range of 4μA while consuming 77.8μA quiescent current.

1.2   Organization

This organization of this thesis is as follows. Chapter 2 gives an overview of a photodiode based sensor and discusses the prior art for current sensing architectures. Chapter 3 discusses the proposed architecture with a brief introduction to VCO based ADCs and design constraints of the prototype circuit. Circuit design details and measurement results are discussed in Chapter 4. Conclusions are drawn in Chapter 5.

CHAPTER 2

PRIOR ART

This chapter describes the various architectures for digital readout circuits which have been proposed in the past. The architecture of such readout circuits depends on the type of sensor it has to be interfaced with. For example, a classical ADC[1] architecture which is designed for a fully differential voltage input will not be suitable for processing a single ended photodiode sensor current with constraints on biasing the diode. To understand more about the design constraints of interfacing with a sensor element, a classical light sensor photodiode is discussed first before delving into the architectural level details of readout circuits.

2.1 Overview of a Photodiode Based Sensor

A classic example of a sensor element is a photodiode, which is a reverse biased diode specifically designed for light sensing applications. Under sufficient reverse

---

[1]Since the distinction between a "digital readout circuit" and an "ADC" is vague, these terms will be used interchangeably throughout the thesis.

bias, it produces an output current (photocurrent) which increases linearly according to the incident light intensity (measured in lux). Since it has a reverse biased P-N junction, the diode has substantially large junction capacitance with large voltage coefficients. The absolute value of the zero bias capacitance mainly depends on the area of the junction.

Figure 2.1 shows the V-I characteristics of the photodiode. I_{PH} is the photodiode reverse current proportional to the incident light and I_{DARK} is the saturation current which is present even without any incident radiation. The saturation cur-
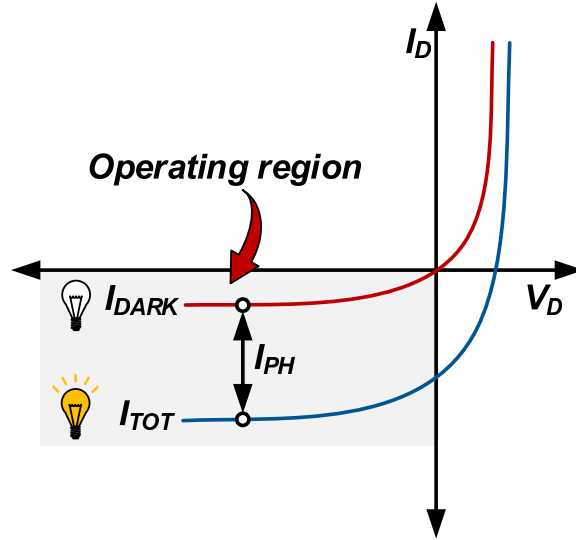
Figure 2.1: V-I characteristics of a photodiode.

rent increases exponentially with the temperature and the junction area of such a diode is usually carefully designed to keep I_{DARK} to a minimum. System level offset removal methods can remove this extra current if required [6].

For an abrupt P-N junction, the junction capacitance of the diode (C_D) typi-

cally varies as,

$$C_D = \frac{C_0}{\sqrt{1 + \frac{|V_D|}{\Phi_i}}} \tag{2.1}$$

where Φ_i is the built in potential of the diode and C_0 is the capacitance with zero bias. Figure 2.2 shows how the capacitance varies with the bias voltage. It can be seen that the capacitance is highly non-linear and hence it is advisable to keep the photodiode bias variation to a minimum.
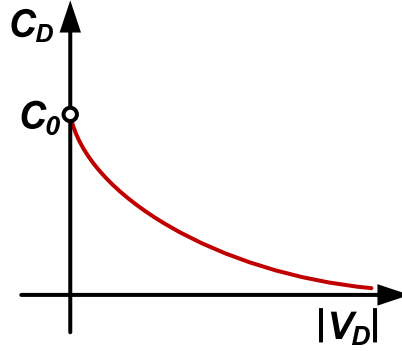
Figure 2.2: Junction capacitance variation for the diode.

Figure 2.3 shows a generic electrical model of such a photodiode sensor. R_{SH}
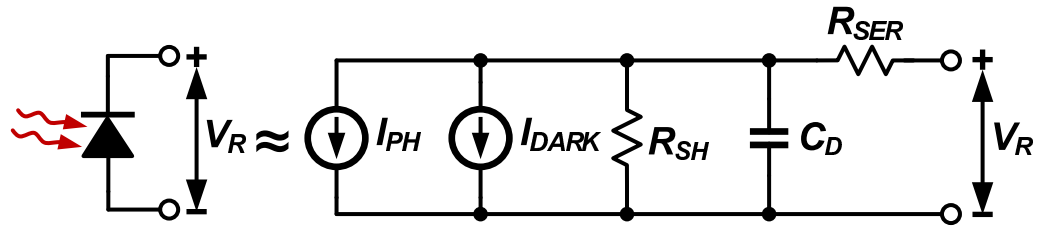
Figure 2.3: Electrical model of a photodiode sensor.

is the shunt resistance which represents the variation of the diode current with applied bias and R_{SER} is the bulk resistance of the diode. With sufficient reverse

bias, R_{SH} is usually of the order of hundreds to thousands of MΩ and R_{SER} is of the order of a few Ω and hence both of them can be safely ignored for design. Dark current is an offset in the conversion process and there are ways to cancel this offset in system level [6]. Consequently, this kind of sensor can be treated as a current source with a non-linear capacitance across it. Even for other types of sensors, for example a piezoelectric sensor, modeling it as a current source (or charge source) with a capacitance across it is a fair assumption without loosing much accuracy [7].

2.2   Current Sensing Digital Readout Circuits

This section discusses various existing current sensing digital readout architectures and briefly describes their advantages and disadvantages. It is assumed the electrical model of the sensor element is as shown in Figure 2.3 irrespective of the type of the sensor.

2.2.1   Transimpedance Amplifier

Transimpedance amplifier (TIA) is used to convert a low level input current to a reasonably high voltage output. A closed loop TIA is essentially a high gain opamp with a large feedback resistor. Figure 2.4 shows the block diagram of a closed loop TIA. The opamp in feedback makes the sensor node, V_C, a virtual ground and the input current is fully diverted to the output. The bias for the sensor is also easily obtained from the virtual short. The voltage domain ADC converts the output

voltage to a digital word, D_{OUT}.
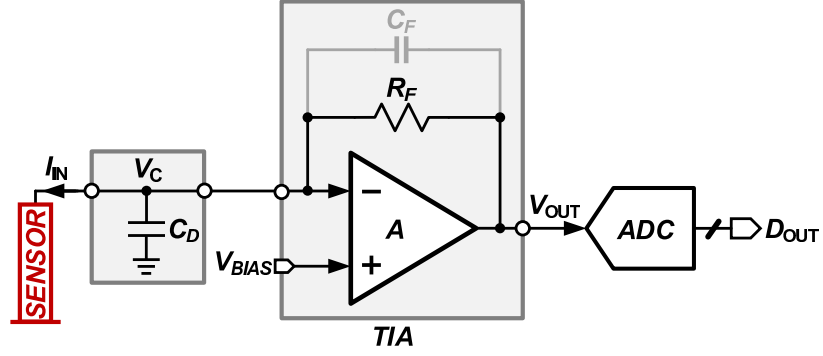
Figure 2.4: Architecture of transimpedance amplifier based readout circuit.

For small signal calculations, TIA looks like a differentiator circuit with large noise gain at high frequency. Hence, a feedback capacitance, C_F, is almost always used to limit the bandwidth of the system. The DC gain of the TIA can be easily calculated as

$$\frac{\mathrm{V_{OUT}}}{\mathrm{I_{IN}}} = \mathrm{R_F} \tag{2.2}$$

The capacitance of the sensor is shown separately for a simpler analysis. In reality the input capacitance of the opamp also contributes to an extra capacitance at the sensor node.

The feedback resistance, R_F, usually consumes large area and the opamp consumes a large current to meet the stability, noise and offset specifications. In addition, the architecture being analog in nature, is not very friendly for process scaling. One advantage of this architecture is that the gain is fairly independent of the sensor capacitance and since the swing at the virtual node is small, the capacitance non-linearity does not affect the performance much. However, for stability,

the total sense node capacitance, feedback resistance, and amplifier bandwidth have to be optmized carefully.

2.2.2 Dual Slope ADC Architecture

Dual Slope ADC belongs to a category of ADC architectures known as "Integrating ADCs" where the output represents the integral of the input over a fixed time period [8]. Figure 2.5 shows the architecture of a dual slope ADC which processes
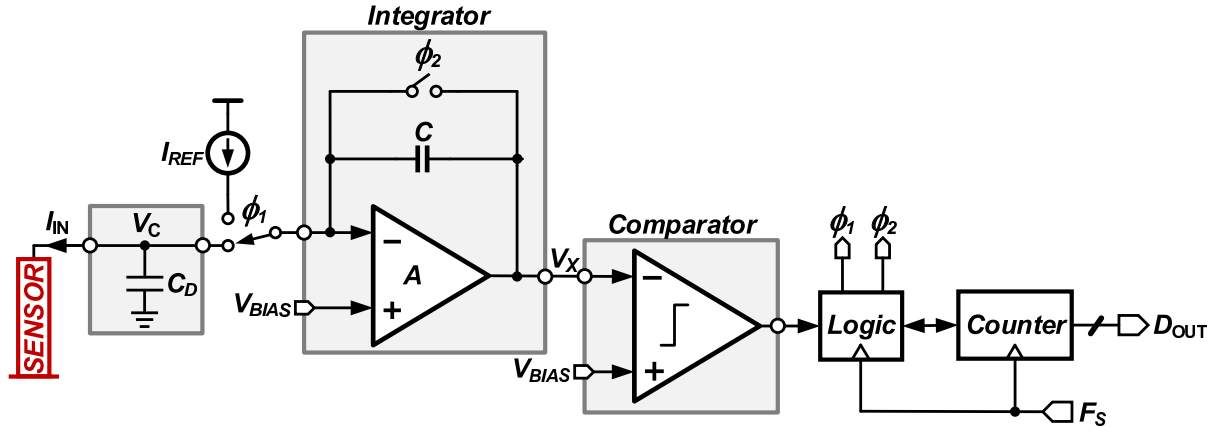
Figure 2.5: Architecture of a Dual Slope ADC based readout circuit.

a current input. The dual slope operation can be easily understood from the integrator output waveform shown in Figure 2.6. There are mainly two phases of operation in a dual slope architecture. In the first phase, the input signal is integrated for a fixed number of clock cycles (usually obtained from an accurate clock source). In the second phase, the integrated output is discharged down using a fixed reference until the comparator output trips. It can be seen the number of clock pulses counted during the second phase is a digital measure of the input. In

some implementations, the first phase might include an auto zero phase where the offset within the system is nulled out. It can be shown that [9] that the number
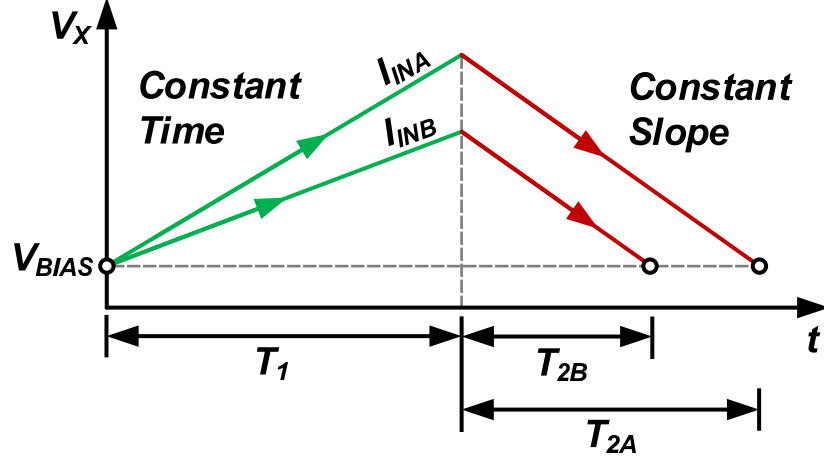
Figure 2.6: Transient waveforms in Dual Slope ADC based readout circuit.

of clock cycles in second phase (T_2) is related to the input signal as,

$$T_2 = T_1 \frac{I_{IN}}{I_{REF}} \tag{2.3}$$

In a dual slope operation, the output does not depend on the feedback capacitance value assuming the value does not change during a single conversion. However, the value of integration capacitance has to be chosen depending on the input current range and clock frequency such that a reasonable value of V_X is obtained without clipping. This makes sure that the noise effects are minimized and the dynamic range of the ADC is maximized. The conversion speed of such an ADC has a strong dependence on its resolution. For an N bit converter, the

worst case conversion time will be,

$$T_{CONV} = 2^{N+1}T_S \qquad (2.4)$$

where T_S is the clock time period. It can be seen that the integrate and self reset behavior of this ADC produces a sinc filtering [9]. So by choosing T_1 carefully, the undesirable components like the power supply ripple (at 60Hz) can be significantly attenuated. Figure 2.7 shows the null locations in the magnitude response of the ADC. In a practical design, errors including capacitor droop due to finite leak-
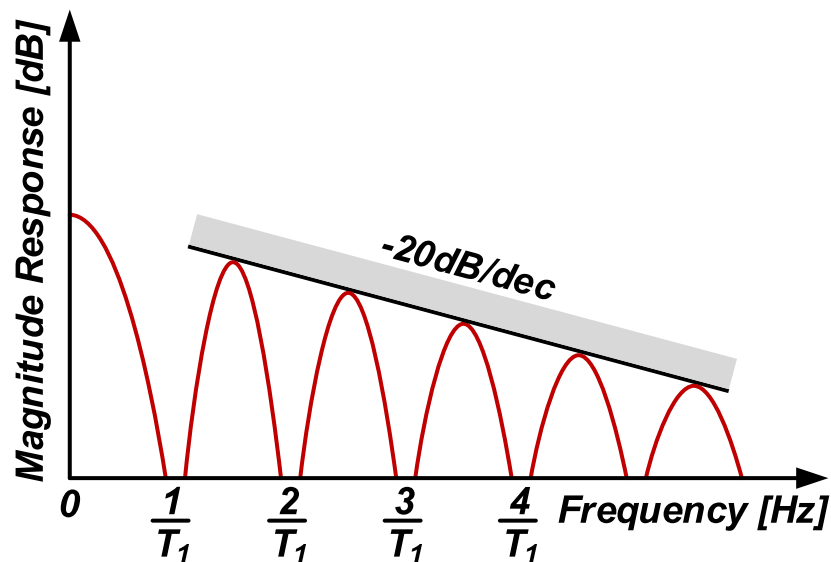
Figure 2.7: Magnitude Response of a Dual Slope ADC.

age, charge injection, non-linearity of integrator and capacitor, and high frequency limitations of the integrator and comparator, need to be accounted for. Design of such integrator opamps and comparators is still a challenge in fine processes.

2.2.3 CMOS Image Sensor Architecture

Figure 2.8 shows a typical CMOS image sensor architecture. In image sensor terminology, this architecture is called an Active Pixel Sensor (APS) because of the presence of an active buffer in the pixel. There are Passive Pixel Sensors (PPS) as well but recent CMOS image sensors employ APS due to its improved performance [1], [10]. The operation of the circuit is demonstrated in Figure 2.9.
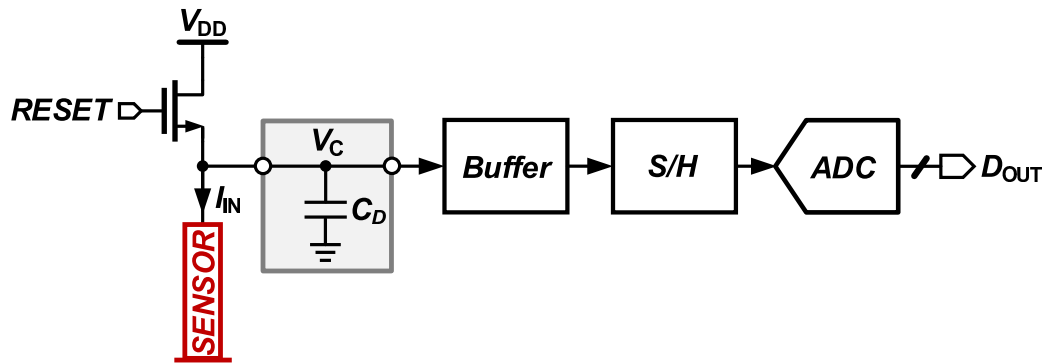
Figure 2.8: CMOS Image Sensor Architecture.

Initially, the sense node, V_C, is reset to a voltage typically close to the supply. After the reset phase, the input sensor current discharges the total capacitance at the sense node for a finite duration with a rate determined by the input current. A sample and hold circuit then samples the voltage at the end of conversion phase which is proportional to the input current. Finally, an ADC converts this sampled voltage into its digital equivalent.

The total capacitance at the sense node includes the sensor capacitance (C_D), input capacitance of the buffer and the parasitic capacitance of the reset transistor. Since the voltage at end of conversion depends on the rate of discharge, the front
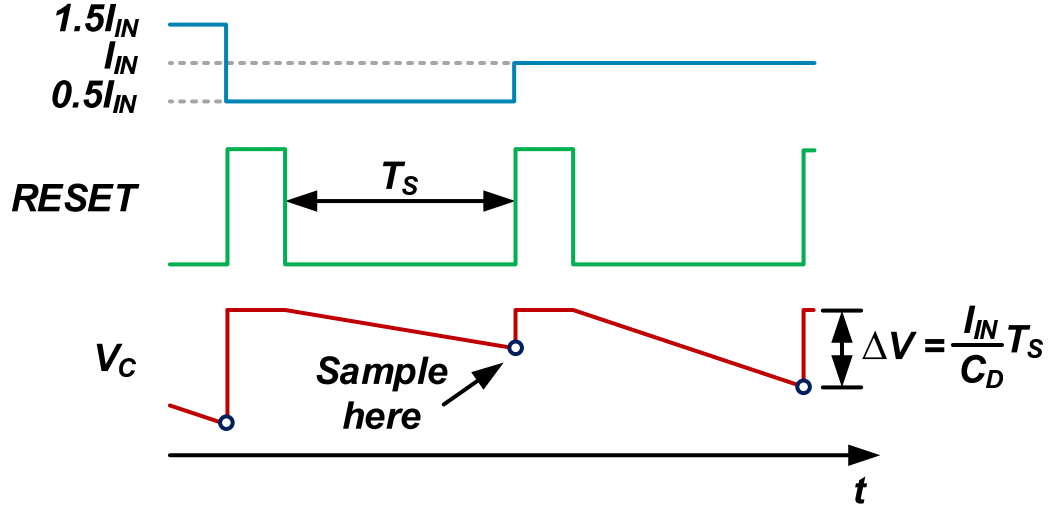
Figure 2.9: RESET and sense node voltage waveforms.

end gain $(\frac{\Delta V}{I_{IN}})$ is dependent on the exact capacitance value. As the voltage swing across the non-linear sensor capacitance changes during a conversion, the effective capacitance is difficult to calculate which results in gain error. More importantly, the variation of C_D with V_C (which in turn is proportional to I_{IN}), leads to an input dependent gain which results in non-linearity. For high dynamic range applications, the conversion time has to be small enough not to saturate the output level but large enough to efficiently use the maximum input range for the ADC.

2.2.4 Pulse Frequency Modulation Architecture

The Pulse Frequency Modulation (PFM) architecture is a technique that is used in many CMOS image sensors to achieve a large dynamic range [5]. Figure 2.10 shows a block diagram of the PFM architecture. Assuming OUT initially goes from 0 to V_{DD}, the sensor current discharges C_D at a constant rate from V_{DD}. Once the sense

voltage crosses V_{BIAS}, the comparator output goes to 0 and resets the sense node again after a very small delay. This results in a self-oscillating structure where the oscillation frequency is controlled by the input current. If the input current increases, the time required for the comparator to trip decreases and the frequency of the comparator output waveform increases linearly. Therefore, if the reset time is small enough, the frequency of the output waveform is linearly proportional to the input current. The comparator output is processed by a Frequency to Digital (FDC) converter which gives out the digital output. Figure 2.11 shows the transient
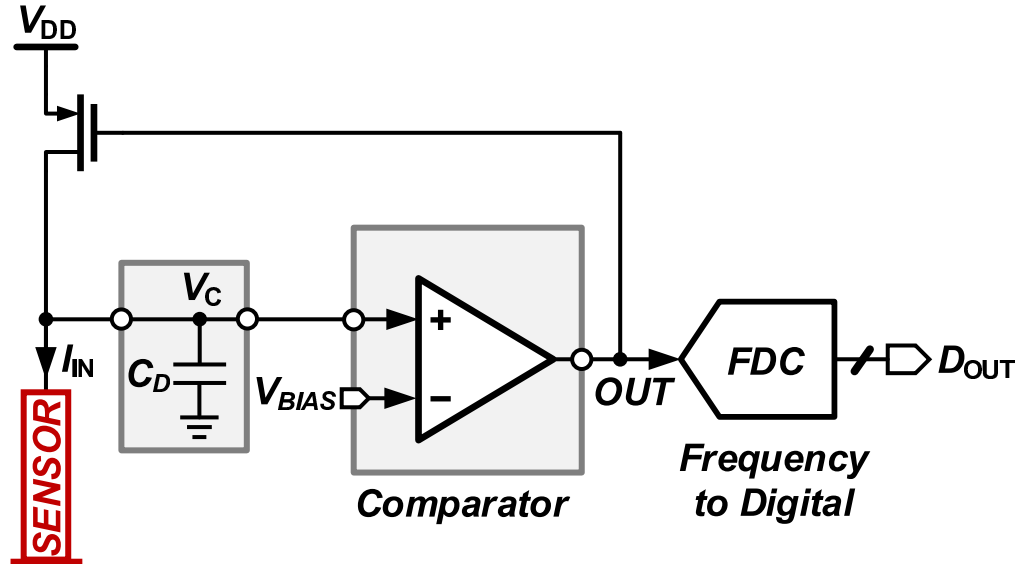
Figure 2.10: Pulse Frequency Modulation Architecture.

waveforms in the PFM circuit with different DC input currents. The frequency at the output of the comparator with a finite reset time is given by,

$$F_{\text{OUT}} = \frac{1}{\frac{C_D(V_{\text{DD}}-V_{\text{BIAS}})}{I_{\text{IN}}} + T_{\text{RST}}} \tag{2.5}$$
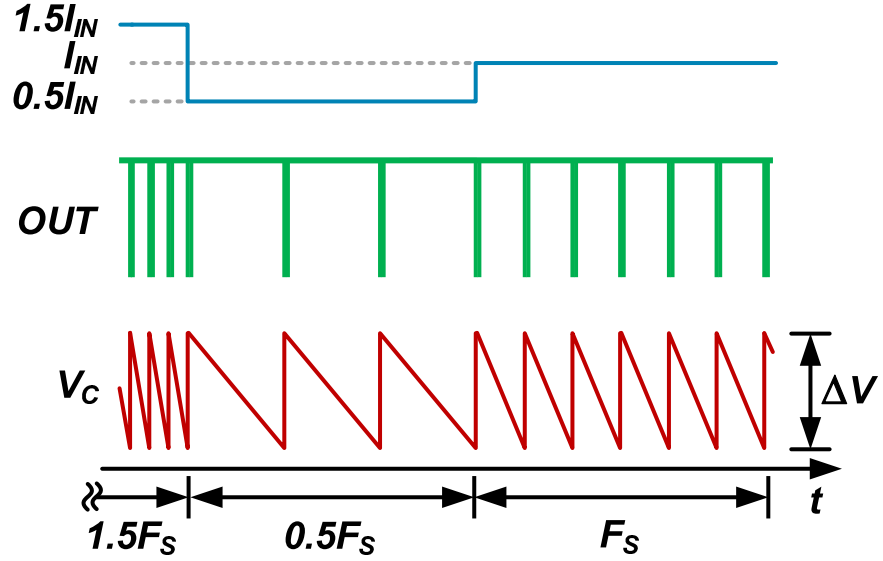
Figure 2.11: Transient waveforms in Pulse Frequency Modulation Architecture.

where T_{RST} is the finite reset time. Reset time mainly includes delays in the comparator and the reset switch. It can be seen that if the T_{RST} is small, the output frequency is linearly proportional to the input current. Figure 2.12 shows the frequency of output vs. the input current. It can be seen that for a large input current, the output frequency saturates to a value dictated by the reset time.

Getting a higher dynamic range from the PFM architecture translates to accurately measuring small to large frequencies. Since FDC can be implemented as a simple counter, extending the counter width (area) is the only penalty in getting more dynamic range. Also since the output frequency scales with the input, the dynamic power consumption also scales with the input current. However, the gain in the conversion process has a strong dependence on the capacitance value. The non-linearity in conversion is significantly reduced compared to the APS architec-
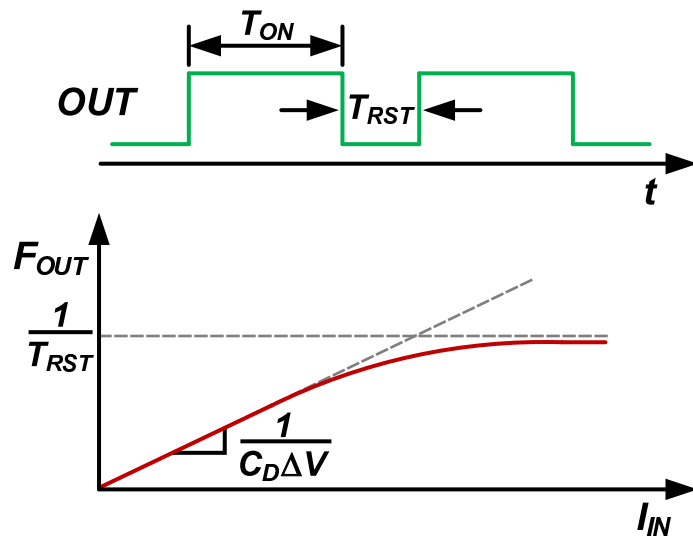
Figure 2.12: Output frequency vs. input current.

ture as the input current does not change the average voltage across the non-linear capacitance. The design of a low power high speed comparator (or zero crossing detector) is still non-trivial with the reduced supply and gain in fine processes.

CHAPTER 3

ARCHITECTURE DESIGN

VCO based ADCs (VCO based Quantizers) [11] have recently emerged as power efficient ADC architectures for many applications. They take advantage of the improved time resolution in finer technology nodes and open loop noise shaping [12]. Circuit techniques to tackle the degradation in performance due to the non-linearity of VCOs are described in [13–15]. Almost all of these designs were implemented for high bandwidth applications with large clock frequency. After a brief overview of the VCO based ADCs, this chapter discusses the proposed digital sensor readout circuit where a VCO based ADC architecture specifically suited for very low bandwidth applications, is used.

3.1 Overview of the VCO Based ADCs

Figure 3.1 shows the conceptual diagram of a VCO based ADC. The input analog voltage, V_{IN}, is converted to a frequency information, F_{OUT}, using a voltage controlled oscillator (VCO). By counting the number of VCO cycles in a fixed time

period, we can get an accurate measure of the VCO frequency. This is implemented using a block called a frequency-to-digital converter (FDC) which converts the frequency information to its digital equivalent. Since the VCO frequency itself is proportional to the analog input, we can see that the digital output represents the analog input to the VCO. Typically, VCOs are implemented using supply controlled or current starved ring oscillators (discussed later).

3.1.1 Small Signal Model

An equivalent small signal block diagram of a VCO based ADC is shown in Figure 3.2. Since the VCO integrates phase continuously (phase is time integral of frequency), it is shown as a continuous time phase integrator where K_{VCO} is the gain (sensitivity) of the VCO in Hz/V. The FDC can be implemented as a phase quantizer or a frequency quantizer. For the purpose of demonstrating noise shaping easily, it shown here as a phase quantizer. The phase is quantized at a sampling rate, F_S. Digital version of the frequency is obtained by passing the quantized phase through a digital differentiator $(1 - z^{-1})$. It can be seen that the
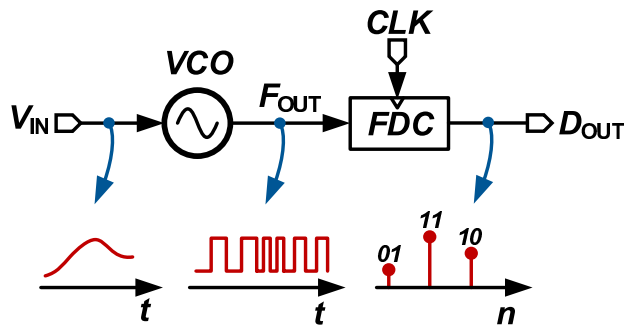
Figure 3.1: Conceptual block diagram of a VCO-based ADC.
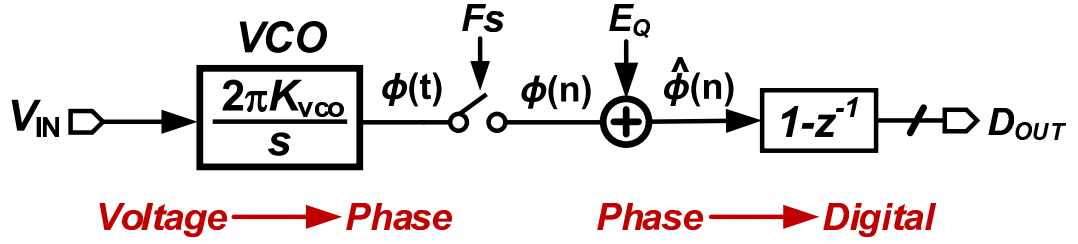
Figure 3.2: Equivalent small signal block diagram of a VCO ADC.

quantization noise, E_Q, gets first order noise shaped as it goes through the digital differentiator. Hence the noise transfer function, NTF of the VCO-based ADC is,

$$\text{NTF}(z) = 1 - z^{-1} \tag{3.1}$$

For frequencies much smaller than the sampling rate, the digital differentiator performs the exact inverse of a continuous integration. Thus the signal transfer function (STF) is just a gain as the signal gets first integrated and then differentiated later in the digital domain. Another advantage of a VCO-based ADC is that it has inherent anti-aliasing much like a continuous time $\Delta\Sigma$ modulator since the signal travels through an integrator before it gets sampled and quantized [16].

For high bandwidth applications, the VCO frequency and the clock frequency are of similar magnitude (usually $\max[F_{\text{VCO}}] \approx \dfrac{F_S}{2}$) and a phase quantizer with a high speed differentiator is used for frequency detection. If input bandwidth is small, a low frequency clock (hundreds of kHz) can be used for saving power. However, using a phase quantizer based approach to extract frequency would necessitate low VCO frequency which is not easy to achieve when implemented with ring oscillator chains with a reasonable K_{VCO} value. In such a case, a counter

based FDC can be implemented as discussed in next section.

3.1.2   Counter Based Frequency Detection

Figure 3.3 shows a practical implementation of a VCO based ADC for low sampling rates. The VCO is implemented as a ring oscillator with 5 stages. The input to
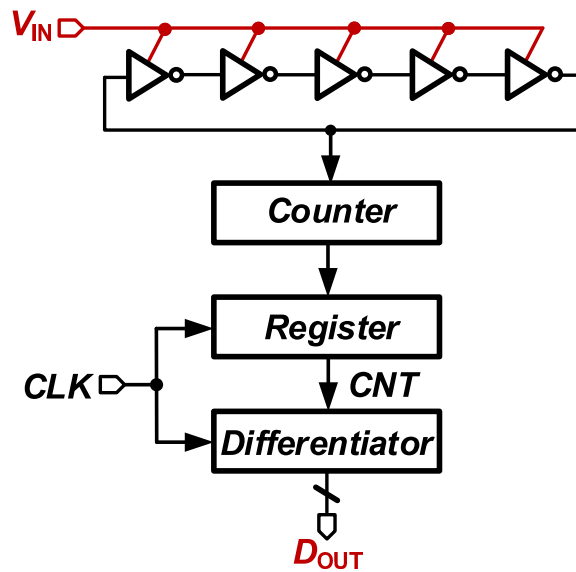
Figure 3.3: Implementation of a VCO based ADC for low sampling rates.

the VCO is the inverter supply itself and the delay of each inverter is dependent on the supply. Hence the output frequency is dependent on the input, though in a non-linear fashion. On every positive edge (or negative) of the VCO output, counter increases its count by one and the register stores the count at the end of the clock cycle. The stored count is a measure of the accumulated phase at the end of that clock cycle. A digital differentiator is used to subtract the stored count values at the end of two consecutive cycles. This gives out the frequency

information in digital representation. In such an implementation, the counter does not have to reset every clock cycle and thus the detrimental effects of finite reset time on noise shaping is eliminated.

Without a reset for the counter, the output of the counter will overflow after
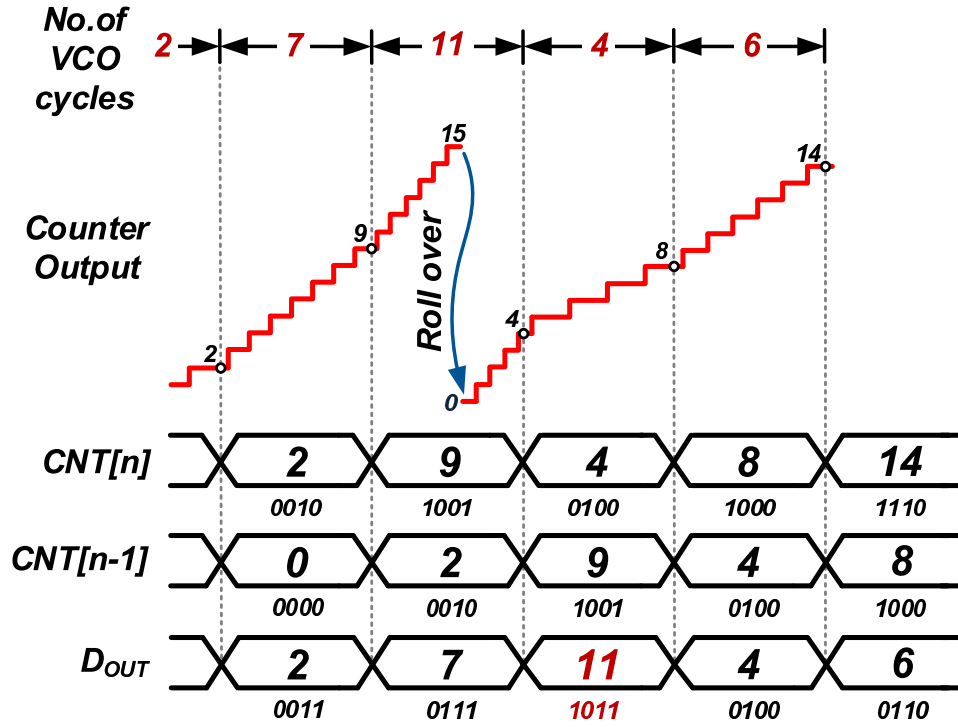
Figure 3.4: Counter with phase wrapping logic

it reaches its highest count. This does not pose a problem if there is only one overflow within a clock cycle, provided 2's complement phase wrapping logic is used. Figure 3.4 shows an example where the 2's complement subtraction is able to retrieve the right frequency output inspite of an overflow. In this example, $D_{OUT} = 11$ represents the case where the digital output is correct even though there was an overflow. Note that there is one clock delay in output due to the

presence of a sampling register.

3.1.3 Gain of a VCO based Quantizer with Counter based FDC

Gain of a VCO based quantizer with counter based frequency detection can be obtained from the small signal diagram shown in Figure 3.5. Since the counter
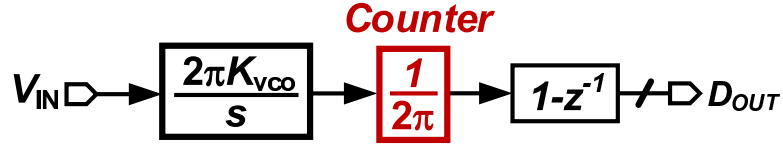
Figure 3.5: Small signal model of VCO based quantizer for gain calculations.

increments its output code by 1 for every 2π radian change in its input, the counter gain is given as $\dfrac{1}{2\pi}$ (code/radian). The digital differentiation can be written as a continuous time differentiation,

$$1 - z^{-1} = 1 - e^{-sT_s} \tag{3.2}$$

where T_S is the clock period. For frequencies much smaller than the clock frequency,

$$1 - e^{-sT_S} = 1 - \left(1 - sT_S + \frac{(sT_S)^2}{2!} + \dots\right)$$
$$\approx sT_S \tag{3.3}$$

Thus the gain of a VCO based quantizer with counter based FDC becomes,

$$A_{VCOQ} \approx K_{VCO}T_S \tag{3.4}$$

To get more insight into the range of values for the gain, we can look at a typical implementation of a current starved ring oscillator as a VCO. This implementation is shown in Figure 3.6. The control voltage, V_C, generates a proportional current,
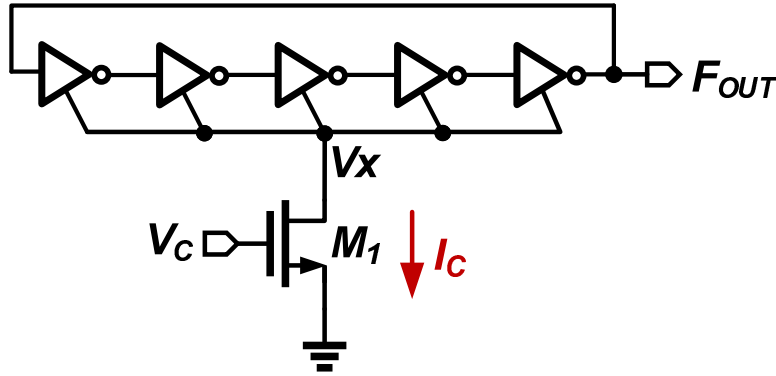
Figure 3.6: nMOS controlled current starved ring oscillator VCO

I_C, which determines the inverter delay. When V_C increases, the current available to discharge the inverter load capacitance, C_L, increases, which reduces the inverter delay or increases the VCO frequency. Let us consider an $N + 1$ bit counter used for the frequency detection such that when the VCO is oscillating with maximum frequency, the FDC gives out a code $= 2^{N+1}$. Assuming the center frequency of VCO is half its maximum frequency, we can write the frequency of the VCO for very small input as,

$$F_{VCO} = 2^N F_S \tag{3.5}$$

Assuming the delay of the inverter is proportional to the time required for C_L to discharge from the supply, V_{DD}, we can write

$$F_{VCO} = \alpha \frac{I_C}{C_L V_{DD}} \qquad (3.6)$$

where I_C (assuming long channel equations are valid) is given by,

$$I_C = \beta (V_C - V_T)^2 \qquad (3.7)$$

Therefore up to a first order approximation, we can write F_{VCO} as,

$$F_{VCO} = \gamma (V_C - V_T)^2 \qquad (3.8)$$

The sensitivity (gain) of the VCO, K_{VCO}, then becomes,

$$K_{VCO} = \frac{\partial F_{VCO}}{\partial V_C} = \frac{2 F_{VCO}}{V_C - V_T} \qquad (3.9)$$

Equation 3.9 shows a strong dependence of K_{VCO} on the frequency of oscillation. So we cannot get arbitrarily large values of K_{VCO} for a fixed value of F_{VCO}. The gain of the VCO quantizer then becomes,

$$A_{VCOQ} = \frac{2^{N+1}}{V_C - V_T} \qquad (3.10)$$

For $N = 4$ and $V_C - V_T = 800\text{mV}$, we have $A_{VCOQ} = 40$. In practical designs, the nMOS transistor might be degenerated for improving noise and linearity. In such

cases and cases where parallel current sources are used across M1 for increasing the center frequency, the gain will be much smaller than the value predicted by Equation 3.10.

A VCO based quantizer with its open loop noise shaping, anti-aliasing property, and performance improvement in finer process, comes out as a power efficient architecture for a digital sensor readout circuit. However, the small DC gain of such an architecture limits the performance when used in a high dynamic range application with a wide range of bias voltages for the sensor. Next section describes an architecture where a method to get infinite DC loop gain for a VCO based ADC operating at low sampling rates, is proposed. The architecture also makes efficient use of the implicit sensor capacitance to get the required performance.

3.2   Proposed Architecture

The conceptual block diagram of the proposed VCO-based sensor current readout circuit is shown in Figure 3.7. A passive integrator, H(s), which is the implicit sensor capacitance, integrates the error current $I_{IN} - I_{DAC}$ and generates voltage V_C. A VCO-based quantizer (VCOQ) digitizes the difference between V_C and the desired sensor bias voltage, V_{BIAS}, and generates digital output, D_F. Because VCOQ exhibits first-order noise shaping, quantization error, E_Q, is shaped by a second-order noise transfer function, thanks to the additional order provided by H(s). While this adequately suppresses E_Q, because of the finite gain of VCOQ, V_C is not forced to be equal to V_{BIAS} in steady state. To circumvent this bottleneck, a
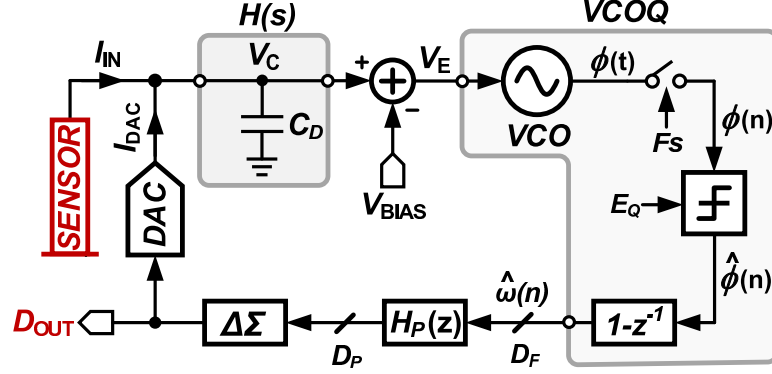
Figure 3.7: Conceptual block diagram of the proposed readout circuit.

digital filter $H_P(z)$ is proposed as shown in Figure 3.7, to provide infinite DC gain so that $V_C = V_{BIAS}$. $H_P(z)$ can be implemented as a simple IIR filter as discussed later. By suppressing variations in V_C, $H_P(z)$ also helps suppress VCOQ non-linearity. To ease hardware complexity, the feedback DAC is implemented using $\Delta\Sigma$ architecture, wherein the digital word (D_P) is first truncated before feeding it to a low-resolution DAC.

3.3 Detailed Architecture

The detailed architecture of the current readout circuit is shown in Figure 3.8. Leveraging the sensor's intrinsic capacitance, passive integrator is realized by feeding the error current, $I_{IN} - I_{DAC}$, into the sense node. The passive integrator capacitance, C_D, includes sensor capacitance and any extra capacitance added at the sense node to minimize ripple on V_C. The VCO is implemented as a cascade of an open-loop transconductor (G_M) and a current-controlled ring oscillator (CCO).
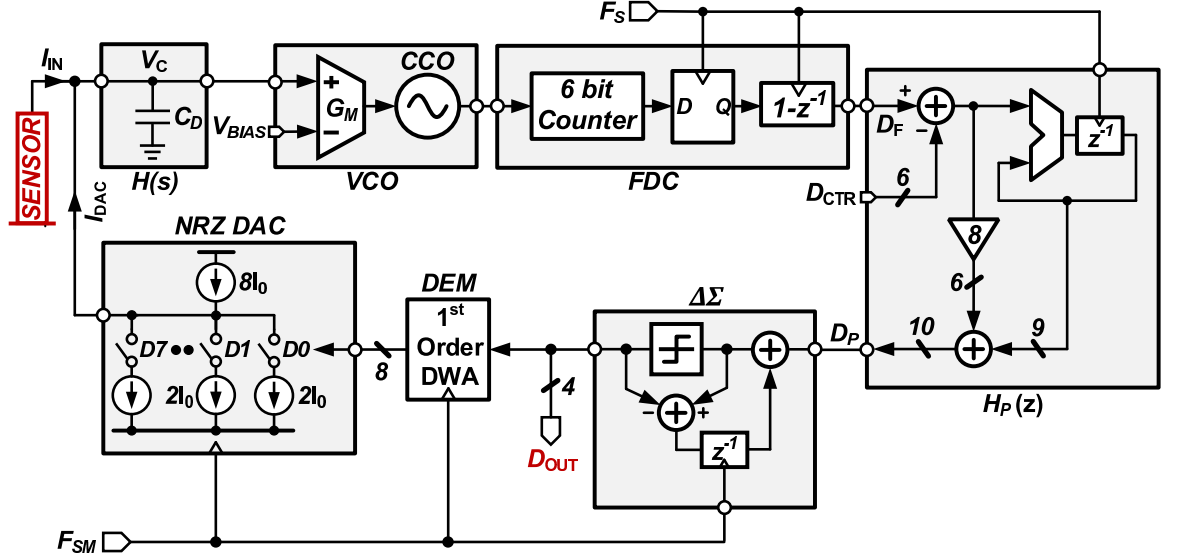
Figure 3.8: Detailed Architecture of the proposed readout circuit.

A Counter-based FDC digitizes VCO output frequency by taking the difference between the number of VCO cycles in two consecutive rising edges of a 160kHz sampling clock, F_S. The $1 - z^{-1}$ block is implemented using two's complement arithmetic, which ensures automatic phase wrapping and obviates the need for resetting the counter on every clock cycle. The FDC output, D_F, is filtered by $H_P(z)$ and fed back to the input through the $\Delta\Sigma$ DAC.

Filter $H_P(z)$ is implemented by an accumulator and a feed-forward path across it. Accumulator provides the high gain needed to force $V_C = V_{BIAS}$ in steady state and the feed-forward path stabilizes the feedback loop that is otherwise unstable because of the presence of two integrators. The feed-forward path gain is set to 8 considering the trade off between the accuracy of V_C and modulator stability. The digital code corresponding to the center frequency of VCO, D_{CTR}, is subtracted

from the FDC output to prevent the accumulator from saturating.

Because $H_P(z)$ output is 10-bit wide in this work, a feedback DAC with more than 1000 levels is needed. Such a DAC occupies a large area and requires very small unit elements that are difficult to implement. For instance, the unit element of a 10-bit thermometric current-mode DAC with $4\mu A$ full-scale current is only 4nA. To overcome these issues, $H_P(z)$ output, D_P, is truncated to 9 levels using a first-order $\Delta\Sigma$ modulator, implemented using error-feedback architecture. The 9 levels are converted to current using a non-return to zero (NRZ) bipolar current-mode feedback DAC. Dynamic element matching (DEM) is used to suppress the DAC mismatch errors. For the truncation error to have negligible impact on the sensor performance, the $\Delta\Sigma$ modulator clock, F_{SM}, is set at 2.56MHz ($\gg F_S = 160$kHz). Performance degradation due to the excess loop delay in the feedback path is negligible as the clock period ($\frac{1}{F_S}$) is very large compared to the delay ($\approx \frac{1}{F_{SM}}$).

3.4 Small Signal Model

The continuous time (CT) small signal model for the proposed readout circuit is shown in Figure 3.9. The differentiator block has been replaced by sT_S. The DAC and $\Delta\Sigma$ blocks are denoted by their gains G_{DAC} and $G_{\Delta\Sigma}$ respectively. $H_P(s)$ is the CT equivalent of $H_P(z)$. We can identify mainly three important transfer functions from this model. First, the gain from input current to output digital code given
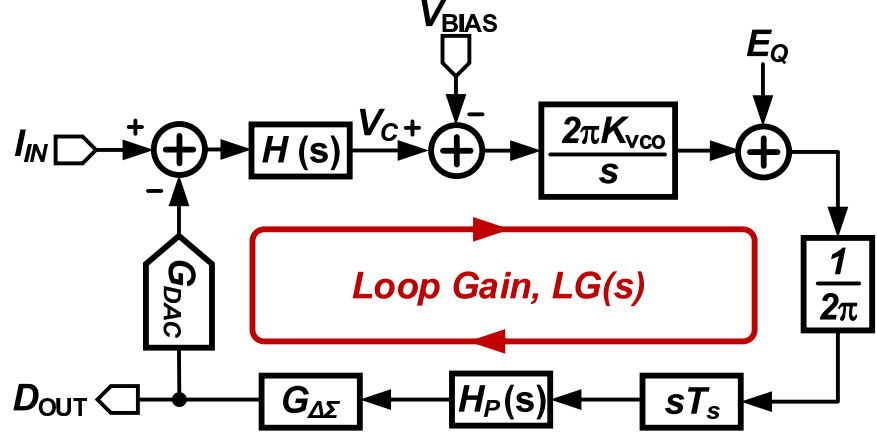
Figure 3.9: Small signal model of the proposed readout circuit.

as,

$$\frac{\text{D}_{\text{OUT}}}{\text{I}_{\text{IN}}} = \frac{1}{\text{G}_{\text{DAC}}} \frac{\text{LG(s)}}{1 + \text{LG(s)}} \tag{3.11}$$

Second, the sensitivity of V_C to input current,

$$\frac{\text{V}_\text{C}}{\text{I}_{\text{IN}}} = \frac{\text{H(s)}}{1 + \text{LG(s)}} \tag{3.12}$$

Third, the sensitivity of V_C to input bias, V_{BIAS},

$$\frac{\text{V}_\text{C}}{\text{V}_{\text{BIAS}}} = \frac{\text{LG(s)}}{1 + \text{LG(s)}} \tag{3.13}$$

where the loop gain LG(s) is given as,

$$\text{LG(s)} = \text{H(s)}\text{H}_\text{P}(\text{s})\text{G}_{\Delta\Sigma}\text{G}_{\text{DAC}}\text{K}_{\text{VCO}}\text{T}_\text{S} \tag{3.14}$$

If the LG(s) is assumed to be large,

$$
\begin{aligned}
\frac{D_{OUT}}{I_{IN}} &\approx \frac{1}{G_{DAC}} \\
\frac{V_C}{V_{BIAS}} &\approx 1 \\
\frac{V_C}{I_{IN}} &\approx \frac{1}{H_P(s)G_{\Delta\Sigma}G_{DAC}K_{VCO}T_S}
\end{aligned}
\tag{3.15}
$$

It can be seen from Equation 3.15 that without the presence of $H_P(s)$ (in such a case, we do not need $G_{\Delta\Sigma}$ as well), the sense node voltage, V_C, would vary depending on the input current. In this particular implementation, $K_{VCO}T_S \approx 27$ and $G_{DAC} = 2\mu A/code$. So for a $4\mu A$ range variation in input, V_C would have changed by 74mV. This is under the assumption that K_{VCO} remains constant over the entire input range of the VCO. But in reality, K_{VCO} would drop down to very low value thereby increasing the deviation of V_C further more. Figure 3.10 shows the variation of V_C in behavioral simulations with and without an accumulator in $H_P(z)$. It can be seen that the accumulator helps in keeping the bias node of the sensor to be a virtual node.

Since the proposed circuit resembles a continuous time $\Delta\Sigma$ modulator with a digital $\Delta\Sigma$ in its feedback path, a discrete time (DT) equivalent model was used to simulate and Figure 3.11 shows an ideal out of band magnitude spectrum obtained using transient simulations in MATLAB. Due to the presence of two integrators, a 2nd order noise shaping is achieved. The out of band spectrum contains nulls at multiples of F_S (160kHz) because of the up sampling operation inside the digital
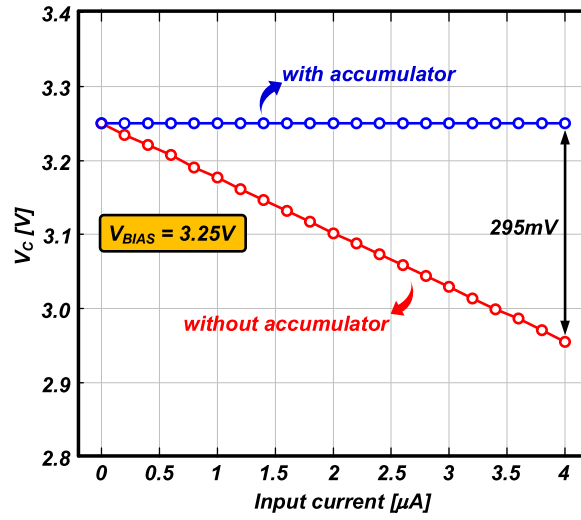
Figure 3.10: Bias node variation with and without accumulator in IIR filter.

$\Delta\Sigma$ modulator. Since the $\Delta\Sigma$ is running at $16F_S$, 8 nulls can be observed within $[0, \dfrac{F_{SM}}{2}]$ as evident from Figure 3.11.
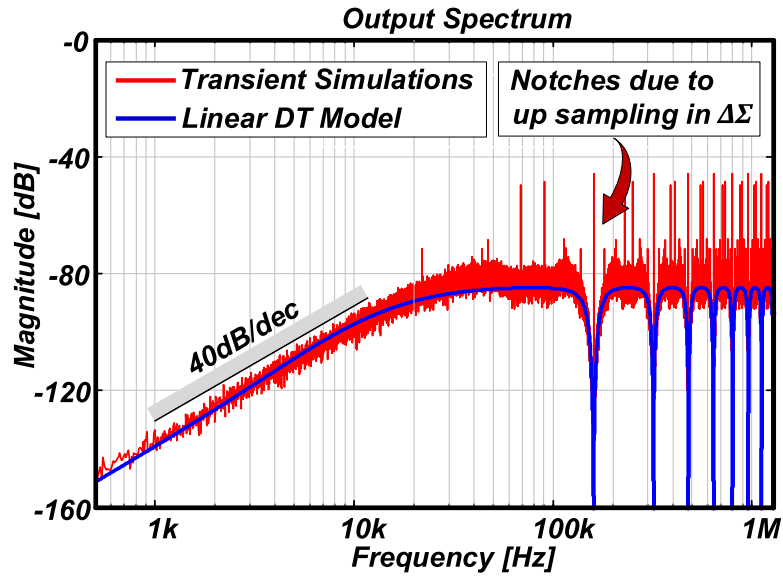
Figure 3.11: Ideal out of band magnitude spectrum.

CHAPTER 4

CIRCUIT DESIGN

This chapter discusses the design of the current controlled ring oscillator VCO, DAC and other blocks. The prototype sensor readout circuit is designed such that it can be interfaced with the photodiode specified in [4]. Since this diode requires around 5V reverse bias, the analog sections of the VCO and DAC are designed with thick oxide devices working at 5V supply and rest of the blocks are designed for 1.8V.

4.1 VCO Design

The schematic of the VCO is shown in Figure 4.1. The G_M stage is implemented as a resistive degenerated nMOS differential pair. The input pair is sized to keep the random mismatch to a minimum. A few mV of offset at the bias of the sensor does not degrade the sensitivity of the sensor element. Hence, extensive offset reduction methods are not needed. A large degeneration resistor is used to increase the linear input range of the VCO hence allowing a wide range of bias

voltages for the sensor interface. The degeneration resistor also helps to reduce the flicker noise contribution of the input pair. However, linearity and lower noise are obtained at the expense of a reduced K_{VCO} since the degeneration resistor reduces the equivalent G_M of the input pair. A dummy circuit is used on one side of the differential pair to make sure that the currents in both the arms match when $V_C = V_{BIAS}$. The VCO delay cells are implemented using CMOS inverters
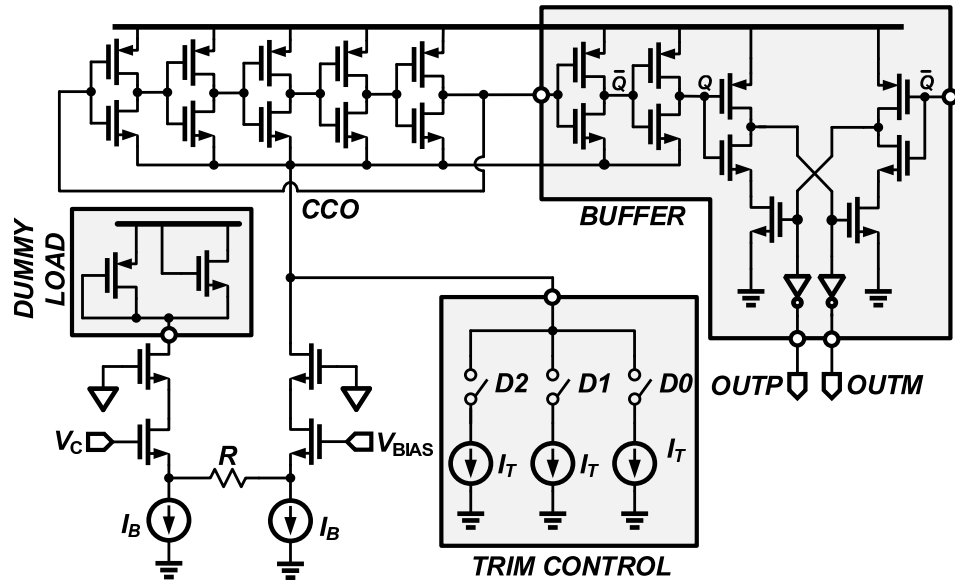
Figure 4.1: VCO and buffer schematic.

that are sized to achieve a center frequency of 2.56MHz with a G_M bias current of 400nA. Fortunately, the VCO phase noise requirement is greatly relaxed due to the presence of an integrator preceding it. An output buffer converts delay cell output to rail-to-rail CMOS levels.

4.2 DAC Design

Figure 4.1 shows the implementation of the feedback DAC. A 9 level current steering architecture is used to implement the feedback DAC. Thermometric implementation is used owing to its inherent monotonicity and ease of implementation with current steering sources. To get large output impedance, cascode devices
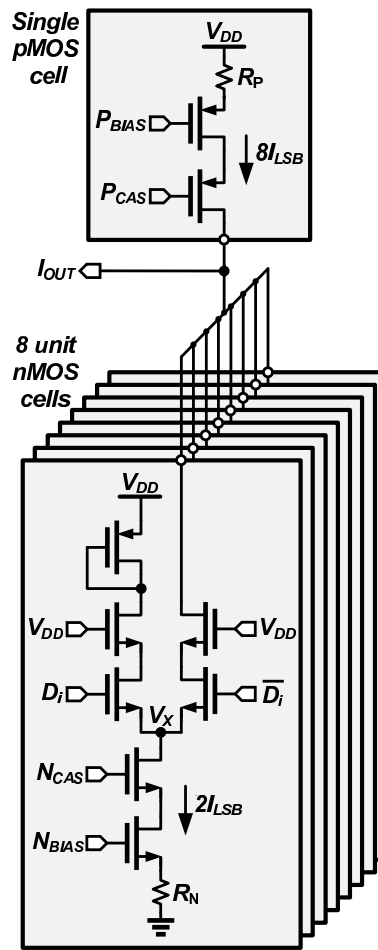
Figure 4.2: DAC schematic.

were used. nMOS cells had more voltage headroom than pMOS cells as the DAC output node in steady state is biased to a voltage close to the supply, V_{DD}. Only the nMOS cells in the DAC switch according to the input while the pMOS side pumps in a constant current. This implementation has less spurious tones (at the expense of more power) than the implementation where both nMOS and pMOS cells switch. Since DAC flicker noise is the major noise contributor in this implementation, large transistors and degeneration resistors are used to keep the noise to an acceptable level. A non return to zero (NRZ) switching scheme is implemented compared to return to zero (RZ) since the performance degradation due to clock jitter in NRZ is smaller.

The DAC is designed as a bipolar implementation which helps to interface the readout circuit with sensors that source or sink current. The clocks for the DAC, DEM and digital $\Delta\Sigma$ are obtained from a 10.24MHz external clock. This high frequency clock is used to generate four phases of 2.56MHz clock which is needed for accurately timing the data from the DAC, DEM and digital $\Delta\Sigma$.

4.3   Digital Design

The digital section involves the FDC, $H_P(z)$ filter, digital $\Delta\Sigma$ and DEM. Standard place and route tools are used to synthesize the digital blocks. The digital $\Delta\Sigma$ is implemented using a first order error feedback architecture. A clock frequency of 2.56MHz is found to be enough to keep the digital truncation noise below the noise floor of the main VCO based quantizer. The presence of a digital $\Delta\Sigma$ modulator

within the global VCO based continuous time $\Delta\Sigma$ modulator loop helps to dither the main modulator to a certain extent.

DEM is implemented using a first order data weighted averaging architecture (DWA). This makes the implementation simple and occupies smaller area compared to a second order DWA. Randomization within DWA is not required as the tones generated do not deteriorate the in-band performance of the readout circuit. The DAC cells are designed for 8 bit matching and the DWA improves the linearity to more than 12 bits.

4.4   Measurement Results

A prototype readout circuit was fabricated in 0.18μm CMOS process and it occupies an active area of 0.36mm^2. The measurement setup is shown in Figure 4.3. Low Dropout Regulators (LDO) are used to generate clean on board supplies from an external 5V supply. Keithley 6221 current source is used to provide an accurate input current. However, the capacitance of the input current source will change the passive integrator transfer function. Fortunately, this only changes the NTF slightly without much degradation in the performance. The output digital data is captured using TLA7000 series logic analyzer from Tektronix and post processing is done using MATLAB.

The DC transfer characteristic, measured with a V_{BIAS} of 3.25V, is shown in Figure 4.4. The prototype achieves an input range of 4μA (limited by the maximum DAC current) with a gain/offset corrected accuracy of 900pA. Below 1nA
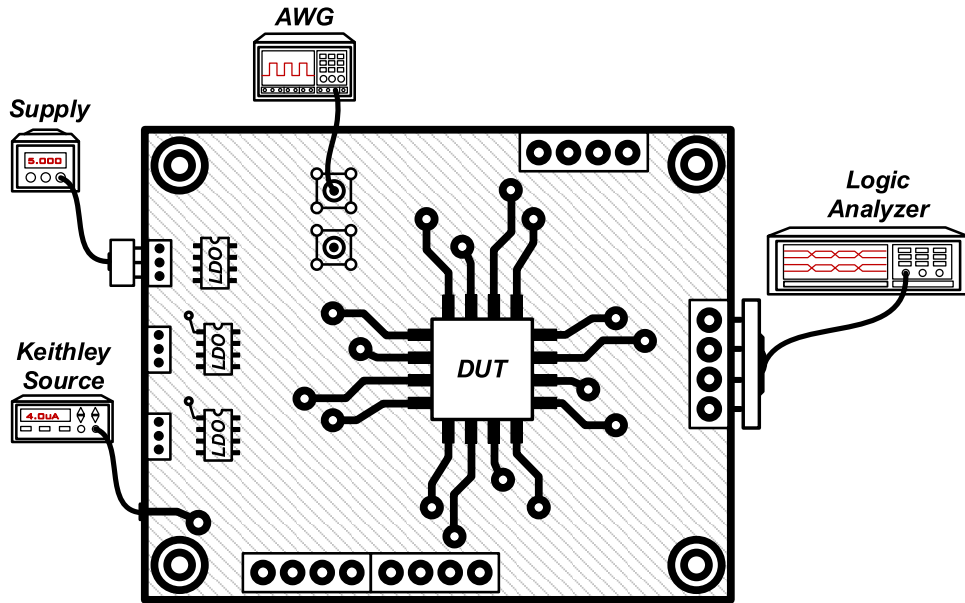
Figure 4.3: Measurement Setup.

input, the resolution is limited by the test setup. Figure 4.5(a), (b), (c) and (d) show measured start-up transient, sensitivity of the error voltage, V_E, to the bias voltage, the ripple on the sensor bias node, and the sensitivity of V_C to the input current, respectively. Thanks to the high DC gain of $H_P(z)$, the sense node always settles to V_{BIAS} independent of the input current. The steady-state ripple is about 10mV, which is largely due to the switching activity of the DAC. The total current consumption is $77.8\mu A$ out of which $62.5\mu A$ is consumed from the 5V supply and $15.3\mu A$ from the 1.8V supply. Table 4.1 summarizes the performance comparison and summary of the proposed readout IC. The die photograph is shown in Figure 4.6.
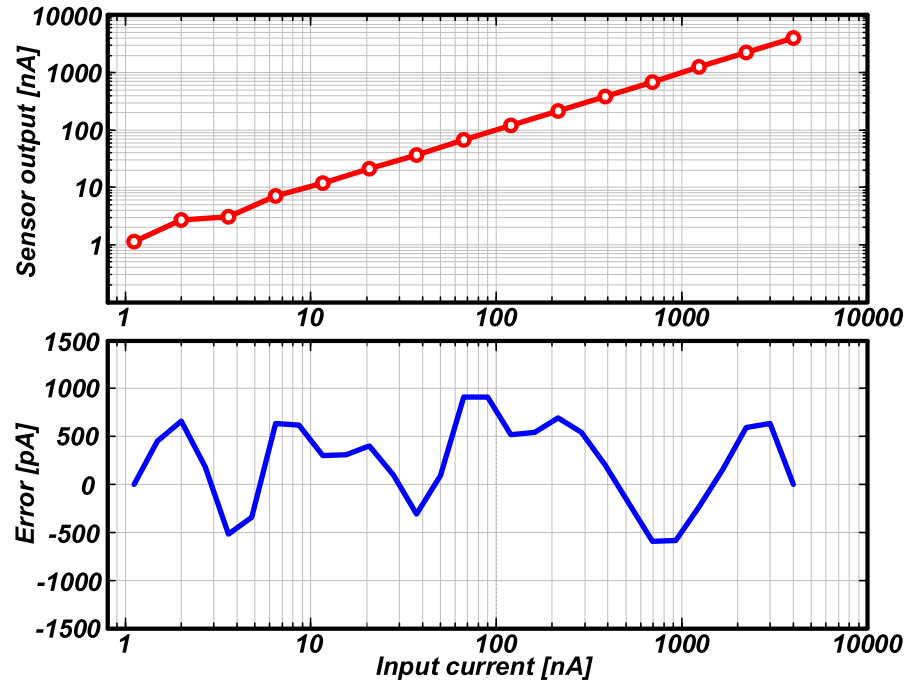
Figure 4.4: Measured DC transfer curve and absolute error plot.

Table 4.1: Performance comparison and summary.

	This work	[17]	[18]
Architecture	Mostly digital	Analog	Analog
Technology [nm]	180	180	180
V_{DD} [V]	5/1.8	1.8	1.8
I_Q [μA]	77.8	1300	110
T_{CONV} [ms]	400	—	—
Area [mm^2]	0.36	1.26	1.69
Input [nA]	1 to 4000	0.004 to 21	1 to 1000
Accuracy [nA]	0.9	0.004	1
Dynamic Range [dB]	73	77	—

Figure 4.5: Measured transient response and bias sensitivity plots

Figure 4.6: Die micrograph of the proposed readout circuit.

CHAPTER 5

CONCLUSION

In this thesis, a new architecture for digital sensor current readout circuit using a VCO based quantizer has been proposed. A major portion of the architecture is digital in nature which can benefit from the improved time resolut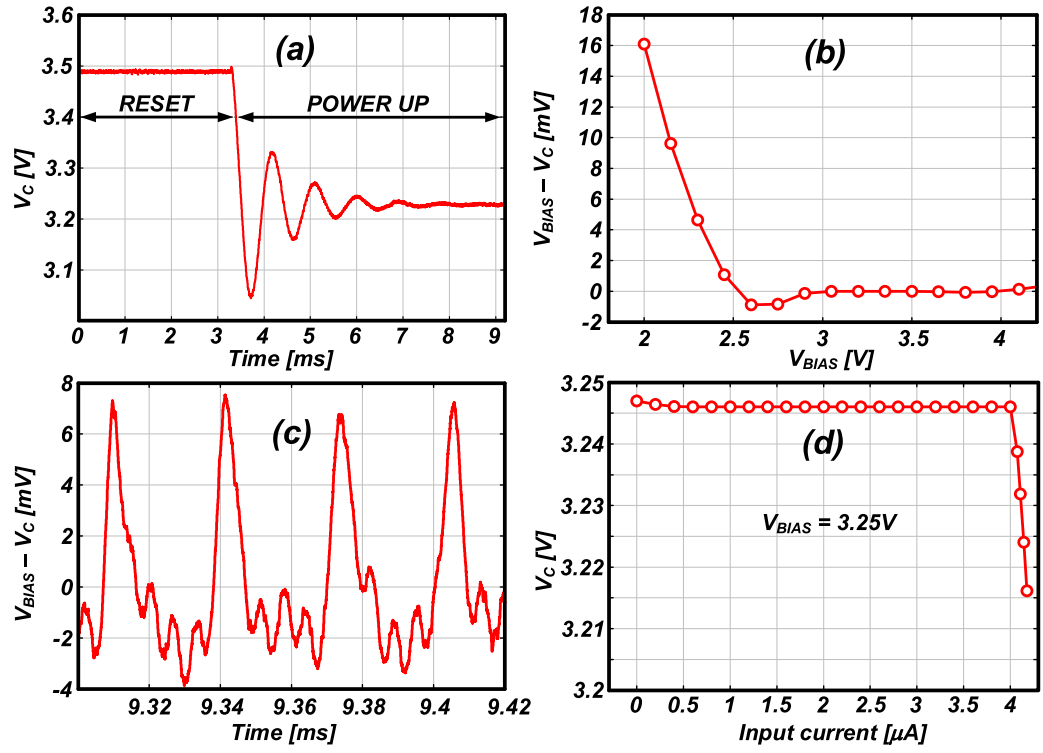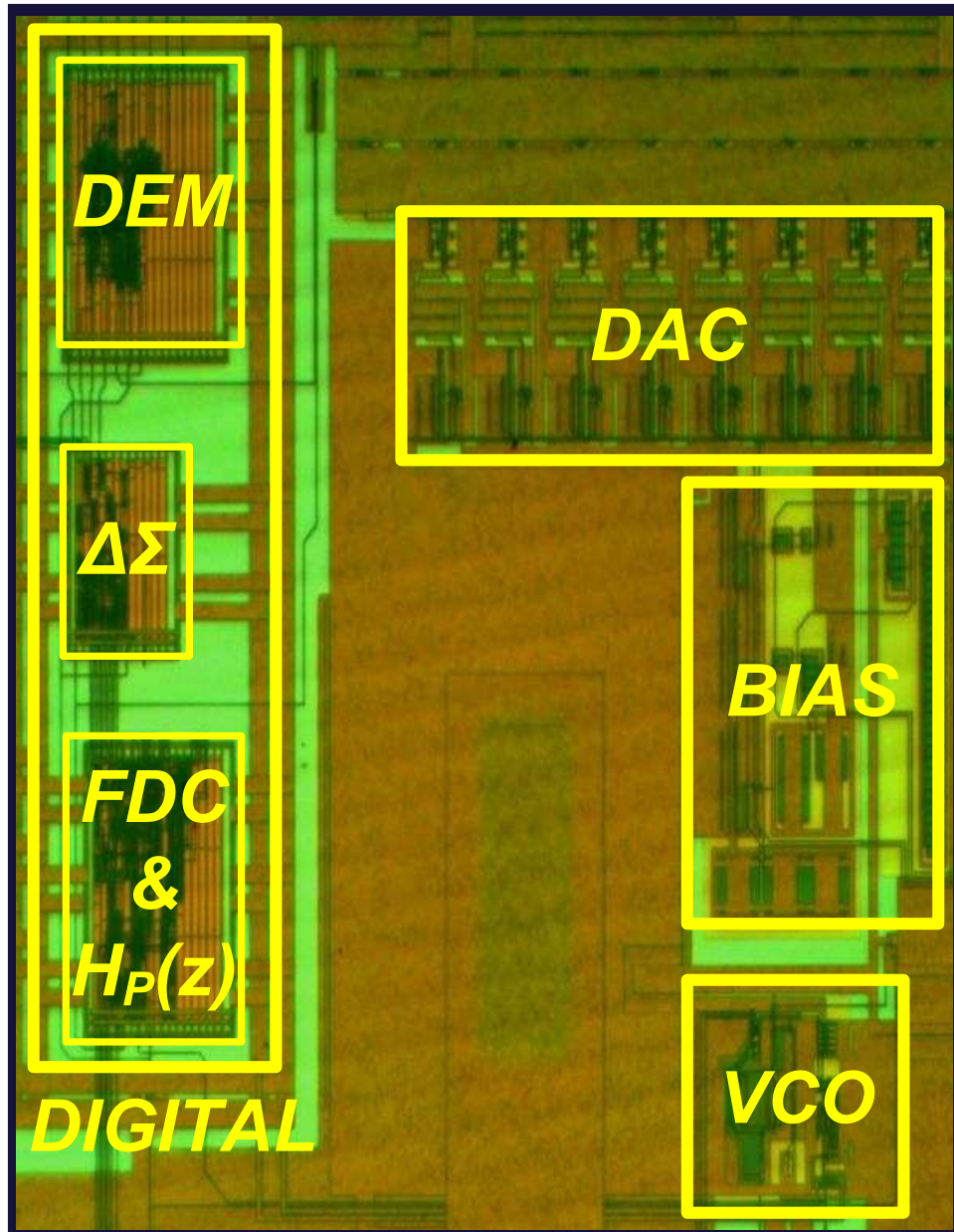ion when implemented in a finer process. The ability of a VCO quantizer to provide open loop first order noise shaping is used effectively to get the required performance. The implicit non-linear capacitance of the sensor is used as a passive integrator to get another order of noise shaping.

To remove the detrimental effects of the finite reset time in counter based FDCs, a counter with a phase wrapping logic is used for the frequency detection. The effectiveness of such a method is demonstrated using an example wherein the FDC is shown to provide accurate results even in the presence of an overflow in the counter.

The finite gain of the VCO quantizer using an nMOS current starved ring oscillator VCO is formulated in a quantitative way in Chapter 3. To tackle this

issue, an architectural technique using a digital IIR filter in the global feedback path, is proposed. The IIR filter is implemented as a simple feedforward gain path and an accumulator. The measured bias sensitivity plots show the efficacy of the proposed IIR filter in increasing the loop gain and thereby reducing the swings at the sensitive nodes. In addition, the reduced swings allow a VCO which is highly non-linear, to be used without the need for extensive linearity improvement techniques. However, the use of an accumulator necessitates a large number of elements in the feedback DAC. This is taken care of, using a $\Delta\Sigma$ DAC wherein the digital output of the filter is truncated before feeding it to a low resolution DAC. Such an architecture is specifically suited for low bandwidth applications as the group delay in a $\Delta\Sigma$ DAC would be too large for a high frequency closed loop implementation.

Compared to the conventional approaches, the proposed architecture does not need a power hungry opamp for maintaining a virtual ground at the sensing node. Measured results from the prototype demonstrates the ability of the VCO based quantizer with an IIR filter feedback to accurately convert the input current to a digital representation. The 5V supply used for the analog sections can be reduced down depending on the application, which will further improve the power efficiency. The digital sections including the FDC, IIR filter, $\Delta\Sigma$, and DEM are coded using a hardware description language and synthesized using place and route tools. Consequently, porting this architecture to a finer process requires little redesign.

Bibliography

[1] E. Fossum, "CMOS image sensors: electronic camera-on-a-chip," *Electron Devices, IEEE Transactions on*, vol. 44, pp. 1689–1698, Oct 1997.

[2] M. Tavakoli, L. Turicchia, and R. Sarpeshkar, "An Ultra-Low-Power Pulse Oximeter Implemented With an Energy-Efficient Transimpedance Amplifier," *Biomedical Circuits and Systems, IEEE Transactions on*, vol. 4, pp. 27–38, Feb 2010.

[3] M. Alhawari, N. Albelooshi, and M. Perrott, "A 0.5V $< 4\mu$W CMOS Light-to-Digital Converter Based on a Nonuniform Quantizer for a Photoplethysmographic Heart-Rate Sensor," *Solid-State Circuits, IEEE Journal of*, vol. 49, pp. 271–288, Jan 2014.

[4] Vishay Semiconductors, "TEMD6010FX01 Datasheet," Rev. 1.8, 20-Aug-12.

[5] X. Wang, W. Wong, and R. Hornsey, "A High Dynamic Range CMOS Image Sensor With Inpixel Light-to-Frequency Conversion," *Electron Devices, IEEE Transactions on*, vol. 53, pp. 2988–2992, Dec 2006.

[6] H.-Y. Cheng and Y.-C. King, "A CMOS image sensor with dark-current cancellation and dynamic sensitivity operations," *Electron Devices, IEEE Transactions on*, vol. 50, pp. 91–95, Jan 2003.

[7] Texas Instruments, "Signal Conditioning Piezoelectric Sensors, Application Report, SLOA033A," Sep 2000.

[8] E. W. Owen, "The elimination of offset errors in dual-slope analog-to-digital converters," *Circuits and Systems, IEEE Transactions on*, vol. 27, pp. 137–141, Feb 1980.

[9] T. C. Carusone, D. A. Johns, and K. W. Martin, *Analog Integrated Circuit Design*. Wiley, 2nd ed., Dec 2011.

[10] B. Fowler, A. El Gamal, and D. Yang, "A CMOS area image sensor with pixel-level A/D conversion," in *Solid-State Circuits Conference, 1994. Digest of Technical Papers. 41st ISSCC., 1994 IEEE International*, pp. 226–227, Feb 1994.

[11] M. Straayer and M. Perrott, "A 12-Bit, 10-MHz bandwidth, continuous-time $\Sigma\Delta$ ADC with a 5-Bit, 950-MS/s VCO-based quantizer," *IEEE J. Solid-State Circuits*, vol. 43, pp. 805–814, Apr. 2008.

[12] J. Kim, T.-K. Jang, Y.-G. Yoon, and S. Cho, "Analysis and Design of Voltage-Controlled Oscillator Based Analog-to-Digital Converter," *Circuits and Systems I: Regular Papers, IEEE Transactions on*, vol. 57, pp. 18–30, Jan 2010.

[13] M. Park and M. Perrott, "A 78 dB SNDR 87 mW 20 MHz bandwidth continuous-time $\Delta\Sigma$ ADC with VCO-based integrator and quantizer implemented in 0.13μm CMOS," *IEEE J. Solid-State Circuits*, vol. 44, pp. 3344–3358, Dec. 2009.

[14] K. Reddy, S. Rao, R. Inti, B. Young, A. Elzhasly, M. Talegaonkar, and P. Hanumolu, "A 16mW 78dB-SNDR 10MHz-BW CT $\Delta\Sigma$ ADC using residue-cancelling VCO-based quantizer," in *ISSCC Dig. Tech. Papers*, pp. 152–154, Feb. 2012.

[15] S. Rao, B. Young, A. Elshazly, W. Yin, N. Sasidhar, and P. Hanumolu, "A 71dB SFDR open loop VCO-based ADC using 2-level PWM modulation," in *Proc. IEEE Symp. VLSI Circuits*, pp. 270–271, Jun. 2011.

[16] G. Taylor and I. Galton, "A mostly-digital variable-rate continuous-time $\Delta\Sigma$ modulator ADC," *IEEE J. Solid-State Circuits*, vol. 45, pp. 2634–2646, Dec. 2010.

[17] R. Heitz, D. Barkin, T. O'Sullivan, N. Parashurama, S. Gambhir, and B. Wooley, "A low noise current readout architecture for fluorescence detection in living subjects," in *Solid-State Circuits Conference Digest of Technical Papers (ISSCC), 2011 IEEE International*, pp. 308–310, Feb 2011.

[18] M. Ahmadi and G. Jullien, "A wireless-implantable microsystem for continuous blood glucose monitoring," *Biomedical Circuits and Systems, IEEE Transactions on*, vol. 3, pp. 169–180, June 2009.